Enhancing Microwave Breast Tomography with Microwave-Induced Thermoacoustic Imaging

Guangran Zhu and Milica Popović

Department of Electrical and Computer Engineering
McGill University, 3480 University Street
Montreal, Quebec Canada H3A 2A7
guangran.zhu@mail.mcgill.ca, milica.popovich@mcgill.ca

Abstract – Finite-element based microwave tomographic system can successfully recover dielectric properties of the human breast, aiming to image malignant breast tissues. When compared with microwave radar imaging, microwave tomography requires simpler electronics and antenna design due to its narrowband operation. However, the narrowband feature limits the resolution of the finite-element mesh often used to recover the dielectric properties of the breast, as there is no *a priori* information for mesh refinement in the critical location within the breast. In this paper, we present a two-dimensional model of a microwave imaging system with monopole antennas and pressure sensors placed in an interleaving arrangement around the breast in its pendant position. The proposed system would synergistically function together with the microwave tomographic modality in a fashion that is envisioned as follows: (1) The system uses a monopole antenna to trigger microwave absorption and, consequently, heating and expansion of the tumor. (2) The array of pressure transducers placed around the breast detect the thermally-induced pressure signals. (3) These signals are used to construct a preliminary breast image. (4) The image is used to generate a non-uniform finite-element mesh, with increased refinement around the suspected tumor locations. (5) The refined mesh is fed to an algorithm utilized by the microwave tomographic system to solve the inverse problem, which will now have *a priori* information and will hence have improved resolution in its resulting image.

Keywords – Microwave tomography, thermoacoustic imaging, breast imaging, FDTD.

I. INTRODUCTION

Human breast imaging has attracted much attention due to the high fatality rate caused by breast cancer. Microwave tomography is one of the imaging techniques for detection of breast tumors. The objective of microwave tomography is to reconstruct the dielectric properties of a body section illuminated with microwaves from a measurement of the scattered field and it can be mathematically described in terms of a non-linear inverse scattering problem [1]. This technique has been applied to image human breasts, most noticeably by Meaney *et al.* [2–5]. The tomographic algorithm developed with these systems belongs to the class of iterative algebraic reconstruction algorithms [6]. The tomographic algorithm assumes that the cross section consists of an array of unknowns in terms of the measured data. The unknowns are initialized with some estimates and the forward problem is solved. Although numerous numerical methods can be used for getting the forward solution, in our work, we focus on the microwave tomographic systems that employ the finite-element formulation. The calculated data are compared with the measurement, yielding some error to assist in updating the unknowns. This iteration continues until the unknowns converge to values that meet a previously defined acceptable threshold. Since knowledge of the breast profile is rarely known *a priori*, the finite-element mesh for the forward problem is uniform. This seriously limits the image resolution and renders the technique not as a screening tool for discovering new lesions.

Thermoacoustic breast imaging is a technique that exploits the heating differential between cancerous tumor and healthy tissue. Depending on the frequency of the electromagnetic wave used to trigger the thermally induced acoustic effect, literature to date reports on optoacoustic (photoacoustic) methods, where the heating is caused by laser illumination [7] and on microwave-induced thermoacoustic methods. Among microwave-induced thermoacoustic imaging systems, Kruger *et al.* reported a design involving 8 waveguides and 128 transducers residing below a pendant breast, showing success in obtaining tomographic images of the breast [8]. Xu and Wang reported a system using unfocused transducers with enhancement in the imaging reconstruction algorithm [9–12]. Recently, Jin and Wang pro-

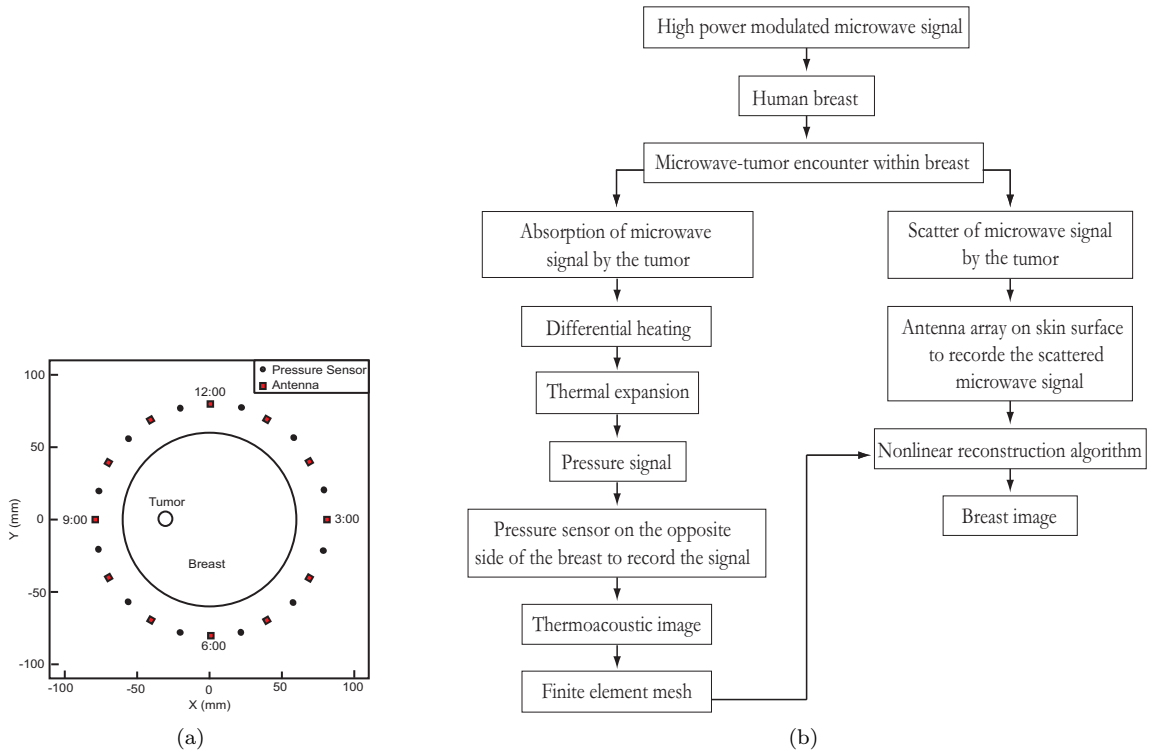

Figure 1: (a) Two-dimensional model of a microwave-based imaging system with monopole antennas and acoustic pressure sensors placed in an interleaving arrangement around the breast in its pendant position. (b) Microwave-induced processes: the flowchart illustrating the thermoacoustic process, resulting from the microwave absorption, and the scattering process.

posed a multi-modality approach, using a pair of ultrasonic transducers to obtain a map of acoustic speed across a breast phantom [13]. Their image reconstruction algorithm, based on the obtained speed map, achieves a signal-to-noise ratio higher than the previous algorithms that assume homogeneity in the acoustic properties of the breast tissue. These studies suggest that microwave-induced thermoacoustic technique may have the capacity to detect early, millimeter-size tumors. Finally, Xu and Wang offered a comprehensive review of the current development in both photoacoustic and microwave-induced thermoacoustic imaging systems [14].

In this work, we present a preliminary study of a system that integrates microwave-induced thermoacoustic imaging with microwave tomography. The system is illustrated in Figure 1 (a). It consists of interleaving monopole antennas and pressure sensors. The system illuminates the pendant breast with a pulse-modulated microwave signal from one antenna. When the pulse encounters a tumor, two processes of interest to our proposed technique happen: (1) Thermoacoustic process is a consequence of microwave absorption as it propagates through the lossy tissues. As the tumor is characterized by a higher electrical conductivity at microwave frequencies, it absorbs more microwave energy and is heated to a higher temperature than the surrounding fatty tissue. The tumor expands thermally and this expansion generates an acoustic (pressure) signal. The pressure signal propagates through the breast and can be detected with the pressure sensors placed around the breast. (2) The scattering process is caused by the dielectric contrast (relative permittivity) between the tumor and healthy breast tissue . The scattered microwave signal can be sensed and collected by the antennas placed around the breast. The location of the microwave transmitter is changed by sequentially using each of the antennas as the source, while other antennas act as passive scatter-collectors, thereby providing several sets of signals. Here, we propose the usage of the signals resulting from the above-mentioned processes in the following manner: the pressure signals can be utilized to construct a preliminary thermoacoustic image and transform the image to a non-uniform, finite-element mesh, which

will then resolve the anticipated tumor locations with more elements. This mesh and the scattered microwave signal are then subjected to the non-linear reconstruction algorithm commonly used in microwave tomographic systems to generate a breast image. The proposed method is illustrated by a flowchart in Figure 1 (b). Unlike a related work that used the ultrasound modality to obtain the preliminary image [15], the here proposed method eliminates the need to have a separate ultrasound source.

An important point on the dielectric data of breast tissue must be addressed here prior to further description of our methodology. A thorough and extremely valuable study on breast tissue parameters was recently reported by Lazebnik *et al.* [16, 17]. Their measurements of samples from normal tissue demonstrate that different composition of the adipose, fibroconnective, and glandular tissue in the sample, inhomogeneous by nature, cause large variations in the dielectric properties, while the previously noted high-permittivity and high-conductivity cancer tissue values at microwave frequencies are consistent with this recent study. This implies that the contrast between the tumor and the glandular tissue surrounding it is not necessarily as pronounced as those assumed in simulation and phantom-based studies to date [18–22]. Nonetheless, these investigations provide valuable insight in the overall underlying principle of microwave breast cancer detection. Similarly, although our work assumes fat-like healthy breast tissue, well contrasted by the tumor in terms of their electrical properties, its main goal is to provide the multi-physics framework for a system that incorporates microwave tomography with microwave-induced thermoacoustic imaging. We also note that the thermoacoustic profile does not provide a detailed image, but rather informs the finite-element mesh generator about the suspect locations where the mesh should resolve the image intended for the microwave tomographic process more finely then elsewhere. For the future model modified according to the newly published data of [16, 17], the higher-conductivity fibroconnective and glandular tissue would also yield finely-meshed suspect locations in the simulation geometry; however, we note again that these locations are simply used to locally refine the mesh but do not instruct the finite-element forward-model to treat them, parameter-wise, in the model as tumors.

This paper focuses on a preliminary computational study of the proposed imaging system. In the next section, we present the modeling of the microwave-induced thermoacoustic process. Section III includes the methodology on the electromagnetic simulation, the artifact removal algorithm, and the algorithm for constructing the preliminary thermoacoustic image. The Specific Absorption Rate (SAR), the computed pressure signals, the thermoacoustic image of the breast, and the non-uniform finite-element mesh are presented in Section IV. In section V, we summarize our findings and offer directions for future work.

II. MICROWAVE-INDUCED THERMOACOUSTIC PROCESS

The thermoacoustic process occurs when the tissue is exposed to electromagnetic radiation. Since there exists a significant contrast in conductivity between normal tissue and breast tumors at certain frequencies, the tumors absorbs more electromagnetic energy. This elevates the tumor temperature and the tumor expands. The mechanical expansion generates pressure signals that propagate to the breast surface, which can be collected by pressure sensors and processed to construct a breast image.

The Pennes' bioheat transfer equation is commonly used to model the heat transfer in perfused tissue, e.g. human breasts,

$$\rho c \frac{\partial T}{\partial t} = \nabla \cdot (k \nabla T) + \rho Q + \rho S - D(T - T_b) \ , \quad (1)$$

where ρ is the tissue density in kgm^{-3}, c is the specific heat capacity in $\mathrm{Jkg}^{-1}\mathrm{K}^{-1}$, T is the local tissue temperature in K, k is the thermal conductivity in $\mathrm{Wm}^{-1}\mathrm{K}^{-1}$, Q is the metabolic heat generation rate in Wkg^{-1}, S is the SAR in Wkg^{-1}, T_b is the temperature of the arterial blood in K, and D is the heat transfer rate that models the heat removal due to blood circulation in $\mathrm{Jm}^{-3}\mathrm{K}^{-1}\mathrm{s}^{-1}$. If the duration of the microwave pulse is short, on the scale of a few micro seconds, the thermal diffusion can be neglected and the Pennes' equation reduces to

$$\rho c \frac{\partial T}{\partial t} = H(\mathbf{r}, t) \ , \quad (2)$$

where H represents the heat deposited into the tissue in $\mathrm{Js}^{-1}\mathrm{m}^{-3}$. In the theory of acoustics, the equation of continuity of mass can be expressed as

$$\frac{1}{B}\frac{\partial p}{\partial t} - \beta \frac{\partial T}{\partial t} = -\nabla \cdot \vec{u} \ , \quad (3)$$

where B is the bulk modulus in Pa, p is the acoustic pressure in Pa, β is the isobaric temperature coefficient of volume expansion in K^{-1}, and $\vec{u}$ is velocity of the differential volume within the mass matter in ms^{-1}. The simple force equation represents the acceleration and deceleration of fluid elements, and it is given by

$$\rho_o \frac{\partial \vec{u}}{\partial t} = -\nabla p \ . \quad (4)$$

Combining (2), (3) and (4) gives the thermoacoustic wave equation

$$\nabla^2 p - \frac{\rho_o}{B}\frac{\partial^2 p}{\partial t^2} = -\frac{\beta}{c}\frac{\partial H}{\partial t} \ . \tag{5}$$

The analytical solution to (5) in 2D, is expressed in terms of the Green's function, which is

$$\begin{aligned} p(\boldsymbol{\rho}, t) &= \int_S g_{2D}(\boldsymbol{\rho}, \boldsymbol{\rho'}, t) \otimes f(\boldsymbol{\rho'}, t) \mathrm{d}S \\ &= \int_S \frac{1}{2\pi} \frac{u(t - |\boldsymbol{\rho} - \boldsymbol{\rho'}|/c_a)}{\sqrt{t^2 - (|\boldsymbol{\rho} - \boldsymbol{\rho'}|/c_a)^2}} \\ &\quad \otimes \left(-\frac{\beta}{c}\frac{\partial H(\boldsymbol{\rho'}, t)}{\partial t} \right) \mathrm{d}S \ , \end{aligned} \tag{6}$$

where $\otimes$ denotes convolution in time, $u(\cdot)$ is the unit step function, and c_a is the acoustic propagation speed in ms^{-1}.

The microwave excitation is a pulse-modulated sinusoidal wave. The heat function can be expressed as

$$H(\boldsymbol{\rho}, t) = \rho S(\boldsymbol{\rho}) I(t) \ , \tag{7}$$

where the temporal illumination $I(t)$ denotes a normalized Gaussian pulse. The SAR, in Wkg^{-1}, is calculated from

$$S(\boldsymbol{\rho}) = \frac{\sigma_e}{2\rho} |\boldsymbol{E}|^2 \ , \tag{8}$$

where σ_e is the electric conductivity in Sm^{-1} and $\boldsymbol{E}$ denotes the electric field in Vm^{-1}.

III. METHODOLOGY

A. Electromagnetic Modeling

We have developed at 2-D TM_z finite-difference time-domain model to simulate the microwave-tissue interaction. The electromagnetic model, shown in Figure 1 (a)), consists of one 120-mm diameter cylinder to mimic the breast cross-section and one 6-mm diameter cylinder to mimic the tumor cross-section. We use deionized (DI) water as the matching medium. The monopole antennas are modeled as infinite-line sources. The computation domain is 200 mm×200 mm, with a uniform grid size of 0.3 mm×0.3 mm and it is truncated with a Perfectly Matched Layer. The single-pole Debye dispersion model is commonly used to approximate the dispersive characteristics of tissue materials. Its expression is

$$\epsilon_r - j\frac{\sigma}{\omega\epsilon_o} = \epsilon_\infty + \frac{\epsilon_s - \epsilon_\infty}{1 + j\omega\tau} - j\frac{\sigma_s}{\omega\epsilon_o} \ , \tag{9}$$

where ϵ_∞ is the relative permittivity at infinite frequency, ϵ_s is the static relative permittivity, σ_s is the static conductivity in Sm^{-1}, and τ is the relaxation time constant in s. We use the Debye parameters of tumor, breast tissue, and deionized water from [22] to calculate their dielectric constants, which are listed in Table 1. Figure 2 shows the dielectric constants over the microwave range. These constants are assigned to the electromagnetic model and we allow a 10% variation in the dielectric constants of the breast tissue over the region to mimic the heterogeneity. For comparison, we show the dielectric constant values both at 6 GHz, frequency used in our previous related work [23] and at 434 MHz, the operating frequency in this paper and in [8].

Table 1: Debye parameters from [22] and the dielectric constants at 434 MHz and 6 GHz [24].

Parameter	Tumor	Tissue	DI Water
ϵ_∞	3.99	6.57	4.55
ϵ_s	54	16.29	77.11
σ_s	0.7	0.23	0.0002
τ (ps)	7	7	7.37
ϵ_r at 434 MHz	53.9818	16.2865	77.0807
σ at 434 MHz	0.7230	0.2345	0.0354
ϵ_r at 6 GHz	50.74	9.8	71.91
σ at 6 GHz	4.82	0.4	6.25

B. Thermoacoustic Modeling

We use the solution expressed in terms of Green's function (6) to numerically compute the pressure signals at particular locations. Table 2 lists the physical properties of the materials recorded in [22, 24]. These parameters are included in (6) to calculate the pressure signals. The normalized Gaussian pulse has a standard deviation of 0.5 µs. Its bandwidth-to-center-frequency ratio is approximately 1/434. Therefore, the distortion in the recorded field magnitude and phase, which will be used in the tomographic system, is considered negligible.

Table 2: Material thermal and mechanical properties [22, 24].

Parameter	Tumor	Average	DI Water
c	3049	2279	4186
ρ	1182	1069	1000
β	9.2×10^{-4}	3.5×10^{-4}	2.07×10^{-4}
c_a	1550	1550	1500

C. Artifact Removal Algorithm

Monopole antennas cause non-uniform heating of the tissue. The tissue close to the antennas is responsible for absorbing the initial, unattenuated microwave energy, and it consequently experiences more heating

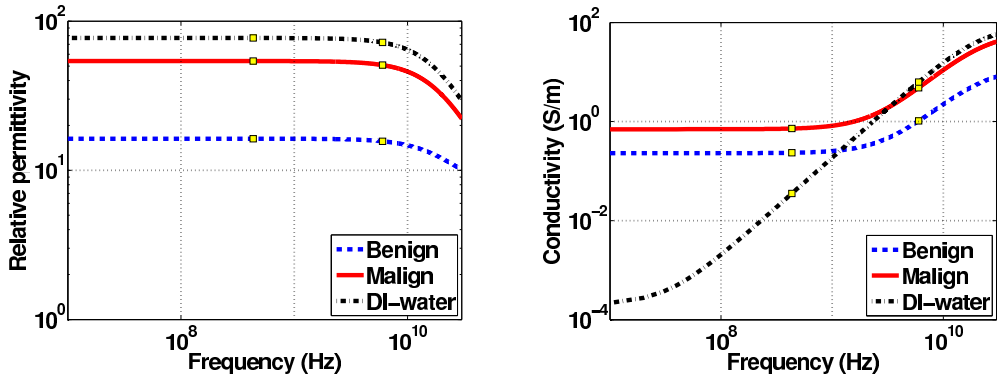

(a) (b)

Figure 2: (a) Relative permittivity and (b) conductivity over the microwave frequency range. [22]

than the rest of the tissue and tumors. The heating-induced artifact is much stronger than the pressure signal due to the heating of tumor and the artifact overshadows the tumor response. We need to eliminate this breast-heating artifact and recover the weak tumor response.

This non-uniform heating happens at all antenna sites and the breast-heating artifacts received on the opposite side of the breast are all similar, but not identical due to the tissue heterogeneity. To remove this artifact, we borrow the skin subtraction method from microwave radar imaging, which removes the reflection of the microwave pulse at the breast-skin interface [25]. This method is based on the assumption that the back-scattered microwave signals from the breast-skin interface contain similar but not identical unwanted artifacts at various antenna sites. The artifact in one signal can be eliminated by a filtered combination of other signals, where the filter weights minimize the mean-squared error between the signal at one antenna and the sum of the filtered signals at all other antenna sites over the portion of the signals dominated by the artifact.

In our scenario, the artifact in the received pressure signal is from the maximally heated tissue, near the transmitting antenna. Assume there are N pressure sensors. Let $p_n(i)$ denote the discrete pressure signal received at the n^{th} pressure sensor at time i. Let $p_1(i)$ be the target signal to be filtered. $\vec{p}_n$ denotes the $(2J+1)\times 1$ vector centered at time i, i.e. $\vec{p}_n(i) = [p_n(i-J)\cdots p_n(i+J)]$. $\vec{w}_n$ denotes the time-independent filter weight applied to $\vec{p}_n(i)$, i.e. $\vec{w}_n = [w_n(-J)\cdots w_n(J)]^T$. Let $\mathbf{p}(\vec{i})) = [\vec{p}_2(i);\cdots \vec{p}_N(i)]$, the concatenated pressure signal from Sensor 2 to Sensor N and $\vec{\mathbf{w}} = [\vec{w}_2;\cdots \vec{w}_N]$, the concatenated filter weights. The optimal weights are calculated from

$$\min_{\vec{\mathbf{w}}} \sum_{i=i_o}^{i_o+M-1} \left| p_1(i) - \vec{\mathbf{w}}^T \vec{\mathbf{p}}(i) \right|^2 , \qquad (10)$$

where the time interval i_o to $i_o + M - 1$ denotes the portion of the signal that contains the breast-heating artifact. The solution to this problem is [26]

$$\vec{\mathbf{w}} = \mathbf{R}^{-1}\vec{\mathbf{P}} , \qquad (11)$$

where $\mathbf{R}$ is the correlation matrix

$$\mathbf{R} = \frac{1}{m} \sum_{i=i_o}^{i_o+M-1} \vec{\mathbf{p}}(i)\vec{\mathbf{p}}(i)^T , \qquad (12)$$

and $\vec{\mathbf{P}}$ is the cross-correlation vector

$$\vec{\mathbf{P}} = \frac{1}{m} \sum_{i=i_o}^{i_o+M-1} p_1(i)\vec{\mathbf{p}}(i) . \qquad (13)$$

The filtered signal from the first pressure sensor is $\hat{p}_1(i) = p_1(i) - \vec{\mathbf{w}}^T\vec{\mathbf{p}}(i)$ and this procedure is repeated for the second pressure sensor being the target signal.

D. Image Reconstruction and Mesh Generation

We use the simple delay-sum algorithm to process the collected pressure signals [18]. The intensity of each pixel Z at location $\boldsymbol{\rho}$ is the energy of the sum of N delayed signals, which is expressed as

$$Z(\boldsymbol{\rho}) = \sum_{i=0}^{M} \left[\sum_{n=1}^{N} a_n p_n(i + \lfloor \frac{|\boldsymbol{\rho} - \boldsymbol{\rho}_n|}{c_a \Delta t} \rfloor) \right]^2 , \qquad (14)$$

where M is the number of discrete time steps, a_n is the weight introduced to compensate for the radial spreading of each cylindrical wave as it propagates outward from the location $\boldsymbol{\rho}$, p_n is the n^{th} pressure signal, Δt is the acoustic time step size, and $\lfloor\cdot\rfloor$ denotes the floor operator.

Given the breast image from the thermoacoustic data, we obtain the contour plot and assign uniform points along each contour to generate the point map. We feed the point map to the DistMesh [27] to acquire the non-uniform, adapted mesh, which can in the next stage of the process be used in the algorithm to solve the inverse problem and generate a more accurate dielectric properties.

IV. RESULTS

Figure 3 (a) shows the SAR over the computation domain under the radiation from the infinite-line source located in the far-right position (3 o'clock). The plot is on the log scale with the peak SAR normalized to 0.4 Wkg^{-1} [28], which is the limit of the ANSI-IEEE Criterion for the average SAR in the whole body. We observe the expected non-uniform heating over the breast area, with pronounced heating in the immediate vicinity of the transmitting antenna. The tumor, due to its high conductivity, also absorbs more microwave energy than its ambient tissue. In two and three dimensions, a cylindrically (spherically) symmetrical source produces one wave that propagates outwardly to the pressure sensor, and at the same time, a second wave that propagates inwardly to the origin. The latter undergoes a reflection at the origin and reappears as an inverted, outwardly propagating wave that eventually reaches the field point. Therefore, the time profile of a photoacoustic wave assumes an N-shape. (In one dimension, the second wave propagates in the opposite direction and will not reach the pressure sensor.) Diebold and Sun presented the solution to the thermoacoustic wave equation (5) of a uniformly-excited homogeneous cylinder under a δ-pulse heating function [29], which is confirmed later by Hoelen and de Mul [30]. This theoretical thermoacoustic signal is shown in Figure 3 (b). Figure 3 (c)-(h) graphs the computed pressure waves at the locations indicated in Figure 3 (a). Our heating-function is a Gaussian pulse with a standard deviation of 0.5 μs, whose spatial span is about 1.5 mm given the constant acoustic speed of 1500 ms^{-1}. This pulse resembles a δ-pulse heating function in comparison to the diameter of the cylinder. Therefore, Figure 3 (c)-(h) all have N-shape traces. The deviation from the theoretical result at different sensor locations is due to the non-uniform heating of the cylinder and heating of the ambient matching background. If the cylinder and the background were uniformly heated, Figure 3 (c)-(h) would assume the theoretic shape regardless of the sensors' locations. The thermoacoustic response of the tumor is also marked in this figure. This tumor response, though, resembles the shape of a differentiated Gaussian pulse since the diameter of the tumor, i.e. 6 mm, is comparable to the spatial span of the heating function.

Due to the high heating of the tissue close to the microwave source, this region generates acoustic waves of high amplitude. The first half of the pressure wave at 2:30 o'clock location in Figure 3 (c) is generated predominantly by the region that is close to the microwave source. As we move the pressure sensor further away from the microwave source, the response generated by the tumor becomes more pronounced with respect to the response of the surrounding tissue, being most noticeable at 10:30 o'clock location in Figure 3 (g), and at 09:30 o'clock location in Figure 3 (h). This suggests that a system based on microwave-induced thermoacoustic imaging may benefit from collecting signals from the pressure sensor placed on the opposite side of the microwave source. In addition, our goal is to apply an algorithm that will remove the artifact of the high-peak pressure signal generated in the immediate vicinity of the transmitting antenna.

In microwave radar imaging, the early breast-skin artifact is separated from the later tumor response in the backscattered microwave signal in time. The time interval parameters i_o and M are carefully chosen to only include the breast-skin artifact. In microwave-induced thermoacoustic imaging, since the pressure wave travels at a significantly lower speed than electromagnetic wave, the breast-heating artifact overlaps with the tumor acoustic response. Therefore, this artifact removal method is applied over the entire range of the pressure signal and the number of consecutive pressure samples weighted before being subtracted from the target signal is bigger than the value used in [25]. In Figure 4, we demonstrate the capability of the artifact removal algorithm when the antenna and the pressure sensor are placed on the opposite sides of the breast. The signals before and after the filtering process are presented. The artifact is clearly removed in all cases, allowing for the tumor response to emerge. We also observe that the filtered signals that contains strong tumor response as in Figure 4 (c) and (d), are less noisier than the signals that contain week tumor response as in Figure 4 (a) and (b).

The delay-sum scheme for image reconstruction has the averaging effect when the noise is added incoherently and the tumor response is added coherently. Therefore, we are still able to recover the tumor in the thermoacoustic image. Finally, Figure 5 shows the thermoacoustic map and the finite-element mesh that contains locally refined elements in the regions that are suspected to contain the tumor. This mesh can now be used in conjunction with the scattered

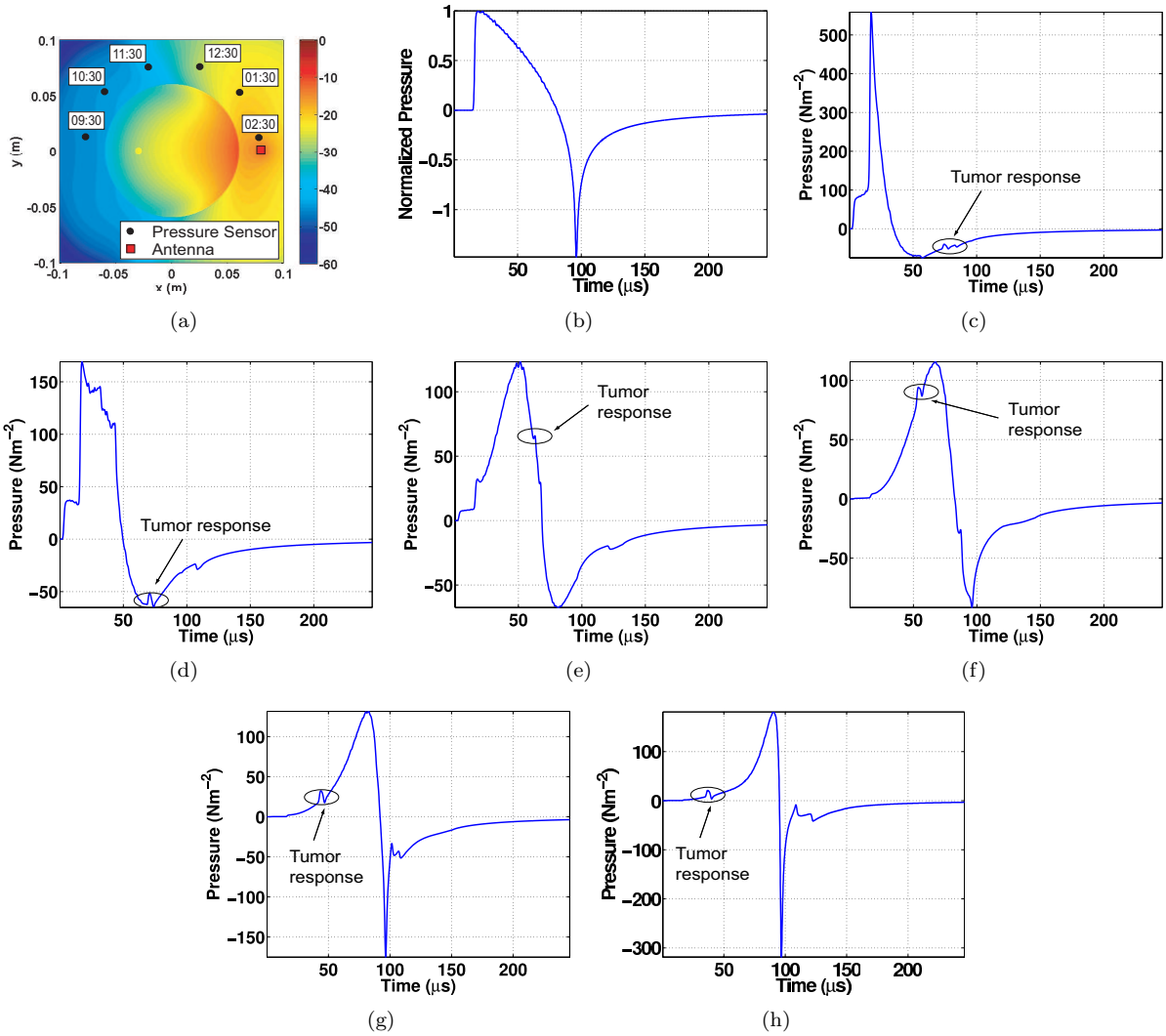

Figure 3: (a) SAR at 434 MHz on a dB scale normalized to 0.4 Wkg^{-1}, with the locations of the antenna (square symbol, at the 3 o'clock location) and pressure sensors indicated by the black dots. (b) Theoretical thermoacoustic signal generated by a uniformly-excited homogeneous cylinder. The trace shows the signal for a δ-pulse heating function. The following graphs show the calculated pressure signals at the sensor locations at the following approximate clock-handle positions: (c) 02:30, (d) 01:30, (e) 12:30, (f) 11:30, (g) 10:30, (h) 9:30.

microwave signals for an improved microwave tomographic image of the breast.

V. CONCLUSIONS AND FUTURE WORK

In this paper, we presented a preliminary study of a breast imaging system that uses microwave-induced thermoacoustic imaging to enhance microwave tomography. Monopole antennas and pressure sensors are interleaved and surround a pendant breast. Monopole antennas are sequentially excited to induce the thermoacoustic process in the breast. The pressure sensors collect signals, which form a thermoacoustic image of the breast. The aim of our paper was to show how an image formed in this fashion can guide the construction of the finite-element mesh which is locally refined to resolve, with more elements, the suspect locations that are likely to contain a tumor. At the same time, the scattered microwave energy is recored at other antennas in terms of magnitude and phase. Therefore, in a complete system, the obtained non-uniform finite-element mesh and the field quantities can be used to recover the

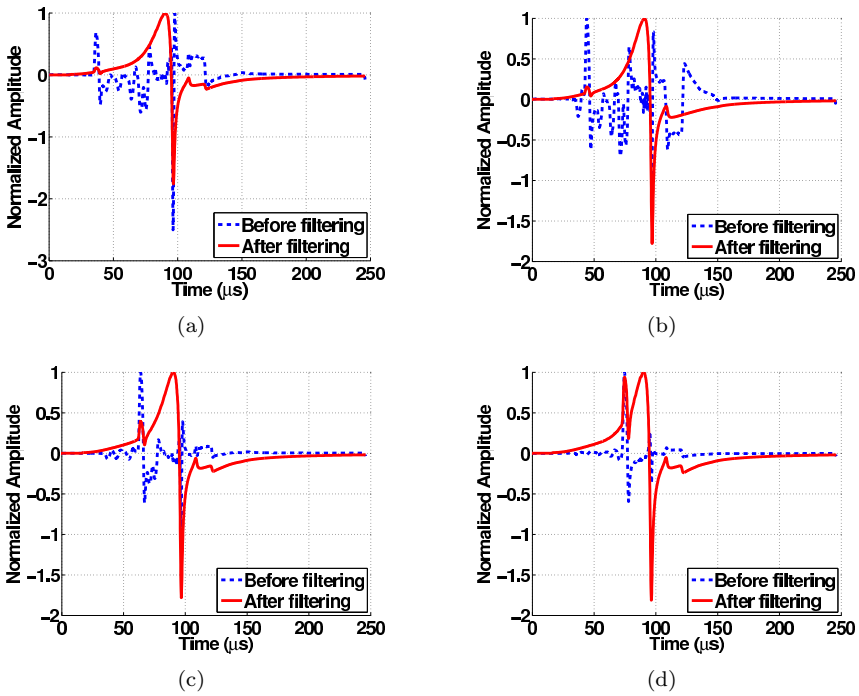

Figure 4: Pressure signals at the side of the breast opposite to the antennas, before and after the removal of breast-heating artifact. Antennas are located at (a) 3:00, (b) 1:00, (c) 11:00, and (d) 9:00 o'clock positions.

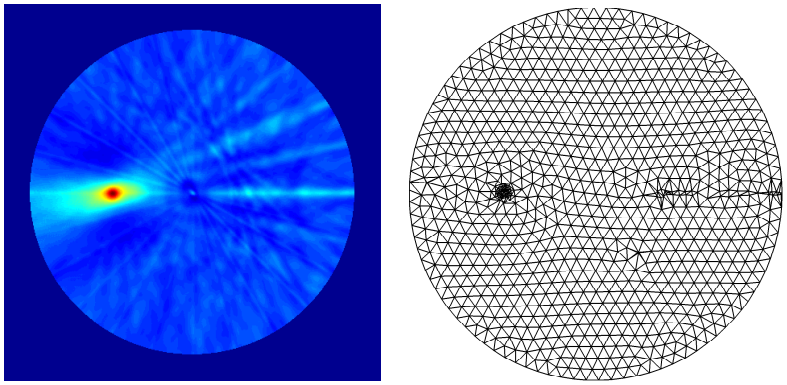

Figure 5: (a) Thermoacoustic map constructed from the pressure signals. (b) Finite-element mesh with local refinement in the region suspected to contain a tumor, to be used for enhancement in the microwave tomographic process.

dielectric properties of the breast. Such a system would overcome the low resolution of microwave tomographic system by providing a finite-element mesh that contains *a priori* information about the potential tumor location. In our preliminary study, we simulated the thermoacoustic process, constructed the thermoacoustic image, and have shown the locally refined finite-element mesh. In the on-going and immediate future work, the more anatomically realistic geometry and tissue parameters as in [16, 17] will be incorporated in the breast model. Further, we are presently implementing an iterative tomographic algorithm to recover the dielectric properties over the non-uniform mesh.

VI. ACKNOWLEDGMENTS

This work was funded by Natural Science and Engineering Research Council (NSERC) of Canada Discovery Grant and by the Le Fonds Québécois de la Recherché sur la Nature et les Technologies (FQRNT) Nouveaux Chercheurs grant.

REFERENCES

[1] A. Broquetas, J. Romeu, J. Rius, A. Elias-Fuste, A. Cardama, and L. Jofre, "Cylindrical geometry: a further step in active microwave tomography," *IEEE Trans. Microw. Theory Tech.*, vol. 39, no. 5, pp. 836–844, 1991.

[2] P. M. Meaney, M. W. Fanning, D. Li, S. P. Poplack, and K. D. Paulsen, "A clinical prototype for active microwave imaging of the breast," *IEEE Trans. Microw. Theory Tech.*, vol. 48, no. 11, pp. 1841–1853, 2000.

[3] P. M. Meaney, K. D. Paulsen, B. W. Pogue, and M. I. Miga, "Microwave image reconstruction utilizing log-magnitude and unwrapped phase to improve high-contrast object recovery," *IEEE Trans. Med. Imag.*, vol. 20, no. 2, pp. 104–116, 2001.

[4] P. M. Meaney, S. A. Pendergrass, M. W. Fanning, D. Li, and K. D. Paulsen, "Importance of using a reduced contrast coupling medium in 2d microwave breast imaging," *Journal of Electromagnetic Waves and Applications*, vol. 17, no. 2, pp. 333–355, 2003.

[5] T. Rubæk, P. M. Meaney, P. Meincke, and K. D. Paulsen, "Nonlinear microwave imaging for breast-cancer screening using gauss-newton's method and the cgls inversion algorithm," *IEEE Trans. Antennas Propag.*, vol. 55, no. 8, pp. 2320–2331, 2007.

[6] A. C. Kak and M. Slaney, *Principles of Computerized Tomographic Imaging.* IEEE Press, 1987.

[7] A. A. Oraevsky and A. A. Karabutov, *Optoacoustic Tomography.* Boca Raton, FL: CRC Press, 2003.

[8] R. A. Kruger, K. Stantz, and W. L. Kiser, Jr., "Thermoacoustic CT of the breast," in *Proc. of SPIE*, L. E. Antonuk and M. J. Yaffe, Eds., vol. 4682. SPIE, pp. 521–525, 2002.

[9] Y. Xu, D. Feng, and L. V. Wang, "Exact frequency-domain reconstruction for thermoacoustic tomography. i. planar geometry," *IEEE Trans. Med. Imag.*, vol. 21, no. 7, pp. 823–828, Jul. 2002.

[10] Y. Xu, M. Xu, and L. V. Wang, "Exact frequency-domain reconstruction for thermoacoustic tomography. II. cylindrical geometry," *IEEE Trans. Med. Imag.*, vol. 21, no. 7, pp. 829–833, Jul. 2002.

[11] M. Xu and L. V. Wang, "Time-domain reconstruction for thermoacoustic tomography in a spherical geometry," *IEEE Trans. Med. Imag.*, vol. 21, no. 7, pp. 814–822, 2002.

[12] ——, "Analytic explanation of spatial resolution related to bandwidth and detector aperture size in thermoacoustic or photoacoustic reconstruction," *Physical Review*, vol. 67, no. 5, p. 056605, May 2003.

[13] X. Jin and L. V. Wang, "Thermoacoustic tomography with correction for acoustic speed variations," *Physics in Medicine and Biology*, vol. 51, no. 24, pp. 6437–6448, 2006.

[14] M. Xu and L. V. Wang, "Photoacoustic imaging in biomedicine," *Review of Scientific Instruments*, vol. 77, no. 4, pp. 1–22, 2006.

[15] H. Jiang, C. Li, D. Pearlstone, and L. L. Fajardo, "Ultrasound-guided microwave imaging of breast cancer: Tissue phantom and pilot clinical experiments," *Medical Physics*, vol. 32, no. 8, pp. 2528–2535, 2005.

[16] M. Lazebnik, L. McCartney, D. Popovic, C. B. Watkins, M. J. Lindstrom, J. Harter, S. Sewall, A. Magliocco, J. H. Booske, M. Okoniewski, and S. C. Hagness, "A large-scale study of the ultrawideband microwave dielectric properties of normal breast tissue obtained from reduction surgeries," *Physics in Medicine and Biology*, vol. 52, no. 10, pp. 2637–2656, 2007.

[17] M. Lazebnik, D. Popovic, L. McCartney, C. B. Watkins, M. J. Lindstrom, J. Harter, S. Sewall, T. Ogilvie, A. Magliocco, T. M. Breslin, W. Temple, D. Mew, J. H. Booske, M. Okoniewski, and S. C. Hagness, "A large-scale study of the ultrawideband microwave dielectric properties of normal, benign and malignant breast tissues obtained from cancer surgeries," *Physics in Medicine and Biology*, vol. 52, no. 20, pp. 6093 – 6115, 2007.

[18] X. Li and S. C. Hagness, "A confocal microwave imaging algorithm for breast cancer detection," *IEEE Microw. Wireless Compon. Lett.*, vol. 11, no. 3, pp. 130–132, 2001.

[19] E. C. Fear, X. Li, S. Hagness, and M. A. Stuchly, "Confocal microwave imaging for breast cancer detection: localization of tumors in three dimensions," *IEEE Trans. Biomed. Eng.*, vol. 49, no. 8, pp. 812–822, 2002.

[20] J. M. Sill and E. C. Fear, "Tissue sensing adaptive radar for breast cancer detection - experimental investigation of simple tumor models," *IEEE Trans. Microw. Theory Tech.*, vol. 53, no. 11, pp. 3312–3319, 2005.

[21] P. Kosmas and C. Rappaport, "Fdtd-based time reversal for microwave breast cancer detection-localization in three dimensions," *IEEE Trans. Microw. Theory Tech.*, vol. 54, no. 4, pp. 1921–1927, 2006.

[22] M. Converse, E. J. Bond, B. D. van Veen, and S. C. Hagness, "A computational study of ultra-wideband versus narrowband microwave hyperthermia for breast cancer treatment," *IEEE Trans. Microw. Theory Tech.*, vol. 54, no. 5, pp. 2169–2180, 2006.

[23] G. Zhu and M. Popović, "2-d computational study of the microwave-induced thermoacoustic effect on human breast with tumor," in *Proc. Annual Review of Progress in Applied Computational Electromagnetics (ACES'07)*, Verona, Italy, Mar. 2007.

[24] F. A. Duck, *Physical properties of tissue: A comprehensive reference book*. San Diego, CA: Academic Press, 1990.

[25] E. J. Bond, X. Li, S. C. Hagness, and B. D. van Veen, "Microwave imaging via space-time beamforming for early detection of breast cancer," *IEEE Trans. Antennas Propag.*, vol. 51, pp. 1690–1705, 2003.

[26] S. Haykin, *Adaptive Filter Theory*, 4th ed. Upper Saddle River, NJ: Prentice-Hall, 2002.

[27] P. olof Persson and G. Strang, "A simple mesh generator in MATLAB," *SIAM Review*, vol. 46, no. 2, pp. 329–345, 2004.

[28] "IEEE standard for safety levels with respect to human exposure to radio frequency electromagnetic fields, 3 khz to 300 ghz," IEEE, Piscataway, NJ, 2006.

[29] G. J. Diebold and T. Sun, "Properties of photoacoustic waves in one, two, and three dimensions," *Acustica*, vol. 80, no. 4, pp. 339–351, 1994.

[30] C. Hoelen and F. de Mul, "A new theoretical approach to photoacoustic signal generation," *Journal of the Acoustical Society of America*, vol. 106, no. 2, pp. 695 – 706, 1999.

Guangran Zhu received the B.Sc. degree in computer engineering and M.Sc. degree in electrical engineering both from University of New Brunswick, Fredericton, Canada in 2003 and 2005. He is currently working towards the Ph.D. degree in the department of electrical and computer engineering at McGill University, Montreal. His research interests include computational electromagnetics, particularly finite-difference time-domain method, microwave-tissue interaction, and related signal processing problems. Mr. Zhu was a recipient of the Graduate Fellowship from IEEE Antenna and Propagation Society in 2007.

Milica Popović received her B.Sc. (1994) from University of Colorado (Boulder, Colorado, USA) and M.Sc. (1997) and Ph.D. (2001) degrees from Northwestern University (Evanston, Illinois, USA), all in electrical engineering. She is currently an associate professor with the Department of Electrical and Computer Engineering at McGill University in Montreal, Canada. Her research interests focus on numerical methods in computational electromagnetics for bio-medical applications, in particular: breast cancer screening with microwaves, wireless implants for physiological research and light interaction with retinal photoreceptor cells. On the teaching side, her efforts include improvement methods for instruction of introductory electromagnetics courses.